Intrinsic Limitation of 2DEG Modulation in GaN-MISHEMT

A. Yesayan, *Member, IEEE*, F. Jazaeri, *Member, IEEE*, B. Parvais, and J. M. Sallese, *Member, IEEE*

***Abstract*—This article presents an analytical model of the barrier layer in GaN-MISHEMT that predicts a limitation of the channel charge density that is expected to reach an asymptotic value under high gate voltages, a feature that was not reported before. We find that this behavior is very sensitive to the device parameters such as the AlGaN barrier thickness, composition, and polarization-induced charge density. Explicit relationships for charge saturation in the quantum well (QW) are proposed and can be used to optimize GaN-MISHEMT architectures.**

***Index Terms*—2-D electron gas (2DEG), AlGaN, AlN, GaN, high-electron mobility transistor (HEMT), MISHEMT, MOSHEMT, polarization charge.**

I. Introduction

HIGH-ELECTRON mobility transistors (HEMTs) made of GaN emerged in the 90s and are still considered as outstanding devices for high-frequency, high-power applications [1], [2], [3], [4], [5], [6], [7], [8], [9], [10], [11], [12], [13], [14], [15], [16], [17], [18], [19], [20], [21], [22], [23], [24], [25]. In contrast to AlGaAs HEMTs, heterostructures based on AlGaN semiconductors host an intrinsic charge sheet layer at the AlGaN/GaN interface due to spontaneous and piezoelectric polarization-induced charges [3], [4], [5], [6], [7], [8], [9]. This fixed charge induces a 2-D electron gas (2DEG) in the quantum well (QW) created by the conduction band discontinuity at the AlGaN/GaN interface. The AlGaN barrier layer can then be undoped, in contrast to AlGaAs HEMTs [26], [27], which has several advantages, such as a higher mobility due to reduced impurity scattering and a lower interface trap density. However, the gate leakage current remains an issue for HEMTs [11], [12], [13], [21], [23] due to the Schottky contact property of the gate electrode. In order to suppress the gate leakage current, the introduction of an additional dielectric layer in form of metal–insulator–semiconductor (MIS) or metal–oxide–semiconductor (MOS) architectures was proposed as it offers significant improvement in terms of gate leakage [14], [15], [16], [17], [18], [19], [20], [21], [22], [23]. In addition, it was reported that adding the gate insulator does not significantly impact the threshold voltage [17]. Still, the introduction of MIS/MOS structures leads to a higher capacitance equivalent thickness (CET) that may reduce the electrostatic control and enhance short-channel effects (SCEs). The threshold voltage variation with the barrier thickness in ungated AlGaN/AlN/GaN heterostructures was studied in [24], and it was outlined that thinner barriers result in a positive shift of the threshold voltage. Thus, the influence of the barrier layer thickness on the device performances is quite critical.

Even though the leakage current issue is mostly resolved in MISHEMTs/MOSHEMTs, the saturation of the transfer characteristics at low drain voltages is still evidenced in literature [17], [22], [23]. Until now, the saturation of the drain current versus gate voltage curves has been mainly attributed to the resistance of the ungated access regions at low drain voltages. However, as we will evidence in this work, the resistance of ungated access regions might not be the only cause for this saturation.

In the following sections, we present a theoretical analysis of the barrier layer-QW system of GaN-MISHEMT and anticipate that for a given barrier thickness and composition, the 2DEG carrier density is expected to become almost independent of the bias at high gate voltages.

Received 1 July 2025; revised 11 September 2025; accepted 12 September 2025. Date of publication 25 September 2025; date of current version 31 October 2025. This work was supported by the Swiss National Science Foundation under Project 200021_213116. The review of this article was arranged by Editor Y. Chauhan. *(Corresponding author: J. M. Sallese.)*

A. Yesayan, F. Jazaeri, and J. M. Sallese are with EDLAB, Ecole Polytechnique Fédérale de Lausanne, 1015 Lausanne, Switzerland (e-mail: jean-michel.sallese@epfl.ch).

B. Parvais is with IMEC, 3001 Leuven, Belgium, and also with the Vrije Universiteit Brussels, 1050 Ixelles, Belgium.

Digital Object Identifier 10.1109/TED.2025.3610338

II. Modeling the Barrier-QW System

A. Device Under Study

We consider an undoped $Al_xGa_{1-x}N$-/GaN-MISHEMT, and we focus on the dependence of the mobile charge density in the QW on the gate voltage. Since we are not interested in calculating the drain current as we restrict the analysis to the MISHEMT "capacitor," we ignore the source and drain.

The polarization-induced positive charge density (σ_{pol}) at the heterointerface generates a 2DEG charge density (n_{2D}) in the QW, making these devices normally-ON. A sketch of a charge distribution in the structure is shown in Fig. 1(a). The schematic band diagrams, where n_{2D} is lower or higher than σ_{pol}, are depicted in Fig. 1(b) and (c), respectively.

In the literature, a constant electric field is often assumed in the undoped $Al_xGa_{1-x}N$ barrier layer [3], [4], [5], [10], [19], [25], [28]. This approximation may be valid when $n_{2D} < \sigma_{pol}$, but we will show that this assumption becomes inapplicable at relatively high overdrive gate voltages, where n_{2D} can exceed σ_{pol} and fails to predict saturation of the 2DEG in the QW. This widely accepted approximation is removed in the present work.

© 2025 IEEE The Authors. This work is licensed under a Creative Commons Attribution 4.0 License.
For more information, see https://creativecommons.org/licenses/by/4.0/

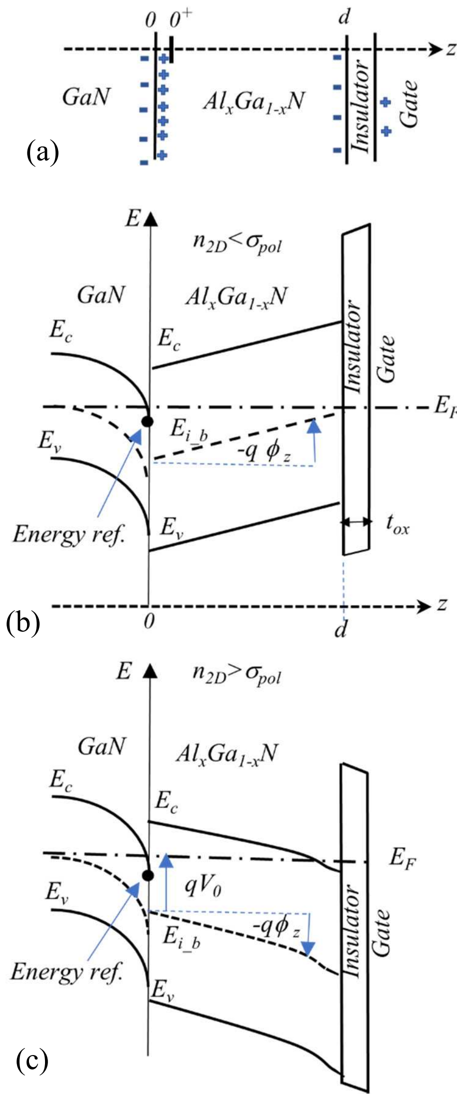

Fig. 1. (a) Illustration of the charge distribution and band diagram for (b) $n_{2D} < \sigma_{pol}$ and (c) $n_{2D} > \sigma_{pol}$.

B. Poisson–Boltzmann Equation in the Undoped AlGaN Barrier

In this section, we solve the Poisson–Boltzmann equation in the barrier and apply the boundary conditions arising from the QW at the AlGaN/GaN interface.

The Poisson equation in the undoped barrier layer is given by

$$\frac{d^2\varphi(z)}{d^2z} = \frac{\rho(z)}{\varepsilon_b} = \frac{q}{\varepsilon_b}(n(z) - p(z)) \tag{1}$$

where $\varphi(z)$ is the electrostatic potential in the $Al_xGa_{1-x}N$ barrier, $\rho(z)$ is the charge density at z, ε_b is the barrier dielectric constant, and $n(z)$ and $p(z)$ are the electron and hole concentrations at z. We assume that $Al_xGa_{1-x}N$ is nondegenerate, meaning that $n(z)$ and $p(z)$ satisfy the Boltzmann statistics

$$n(z) = n_{i_b}\exp\left(\frac{E_F - E_{i_b}(z)}{kT}\right) \tag{2a}$$

$$p(z) = n_{i_b}\exp\left(-\frac{E_F - E_{i_b}(z)}{kT}\right) \tag{2b}$$

TABLE I
MATERIAL PARAMETERS USED IN THE MODEL

Sym.	GaN	$Al_xGa_{1-x}N$	$In_{0.1}Ga_{0.9}N$
N_c (cm^{-3})	$2.3\cdot10^{18}$	$(1-x)N_{C_{GaN}} + x\cdot N_{C_AlN}$	$2.2\cdot10^{18}$
N_v (cm^{-3})	$2.3\cdot10^{19}$	$(1-x)N_{V_GaN} + x\cdot N_{V_AlN}$	$1.8\cdot10^{19}$
E_g (eV)	3.42	$x\cdot E_{g_{AlN}} + (1-x)\cdot$ $\cdot(E_{g_{GaN}} - b\cdot x)$, $b = 0.5$ [31]	3.02
ΔE_c (eV)	-	$0.75\cdot(E_{g_AlGaN} - E_{g_{GaN}})$, [32]	0.26 eV
χ (eV)	3.86	3.86-0.75*ΔE_g	4.15
m_{eff}/m_o	0.22	0.25	0.19
ε_{rel}	8.9	8.9-0.4·x	9.3

where E_F is the Fermi level (constant in the z-direction since no current flows across the heterostructure in the equilibrium), n_{i_b} and $E_{i_b}(z)$ are the intrinsic carrier density and intrinsic Fermi level in the barrier, and other symbols having their usual meaning. Note that the assumption of nondegeneracy is valid if the mobile charge density is lower than the effective density of states (the values of the effective density of states for the conduction band (N_c) and valence band (N_V) are listed in Table I).

In our analysis, we consider that the QW is populated with electrons, meaning that the Fermi level stands "close" to the ground state of the QW, i.e., in the vicinity of the conduction band edge of GaN, $E_F > E_{i_b}(0)$. In addition, the intrinsic carrier density in GaN and AlGaN, calculated at 300 K with the data presented in Table I, is as low as 10^{-10} and 10^{-16} cm^{-2}, respectively, meaning that according to relation (2b), holes can be neglected in (1).

For simplicity, the energy reference is taken as the conduction band edge of GaN at the heterointerface, $E_{c_GaN}(0) = 0$. According to the band diagrams in Fig. 1, the intrinsic Fermi level is given by

$$E_{i_b}(z) = \Delta E_c - \frac{E_{G_b}}{2} + kT\ln\left(\frac{N_{V_b}}{N_{C_b}}\right) - q\varphi(z) \tag{3}$$

where ΔE_c is the conduction band offset between AlGaN and GaN, E_{G_b} is the bandgap of the AlGaN barrier layer, N_{C_b} and N_{V_b} are the conduction and valence band effective density of states of the barrier layer, and $q\varphi(z)$ is the band bending, see Fig. 1(b) and (c) and Table I for the parameters. Note that $\varphi(z)$ is positive in Fig. 1(c).

Introducing (3) in (2a), relation (1) can be rewritten as

$$\frac{d^2\varphi}{d^2z} = \frac{q}{\varepsilon_b}n_{i_b}\exp\left(\frac{\varphi(z) - V_o(n_{2D})}{U_T}\right) \tag{4}$$

where the potential $V_o(n_{2D})$ is defined by

$$qV_o(n_{2D}) = \Delta E_c - \frac{E_{G_b}}{2} + kT\ln\left(\frac{N_{V_b}}{N_{C_b}}\right) - E_F(n_{2D}). \tag{5}$$

The potential $V_o(n_{2D})$ depends on the difference between the intrinsic Fermi level and the Fermi level at $z = 0$, see Fig. 1(c) (V_o takes negative values). The Fermi level is uniquely linked to the 2-D charge density n_{2D} (see the Appendix for details),

which justifies the implicit dependence of V_o on n_{2D}

$$E_F(n_{2D}) = kT \ln\left(\exp\left(\frac{n_{2D}}{\mathrm{DOS}kT}\right) - 1\right) + \gamma n_{2D}^{\frac{2}{3}}. \quad (6)$$

We rewrite relation (4) by multiplying each member by $(d\varphi(z)/dz)$ to obtain

$$\frac{d}{dz}\left(\frac{d\varphi(z)}{dz}\right)^2 = \frac{2qn_{i_b}}{\varepsilon_b}\exp\left(\frac{\varphi(z) - V_o(n_{2D})}{U_T}\right)\frac{d\varphi(z)}{dz}. \quad (7)$$

Integrating (7) from $z = 0^+$ [corresponding to AlGaN/GaN interface from the AlGaN side, see Fig. 1(a)] to any coordinate z in the barrier, the electric field $F_b(z)$ depends uniquely on the local potential $\varphi(z)$ once the potential and the electric field at $z = 0^+$ are known, namely, $\varphi(0^+)$ and $F_b(0^+)$

$$F_b(z) = \mp\sqrt{\alpha e^{\frac{\varphi(z)-V_o(n_{2D})}{U_T}} - \alpha e^{\frac{\varphi(0)-V_o(n_{2D})}{U_T}} + (F_b(0^+))^2} \quad (8)$$

where $\alpha = 2(qn_{i_b}/\varepsilon_b)U_T$.

Considering a Gauss surface passing through $z = 0^+$ [see Fig. 1(a)], the electric field in the barrier at $z = 0^+$ is

$$F_b(0^+) = q(\sigma_{\mathrm{pol}} - n_{2D})/\varepsilon_b. \quad (9)$$

From (9), the sign of the electric field in the barrier layer is defined by the imbalance between the charge density in the QW with respect to the polarization charge density. The sign in relation (8) will then depend on whether $F_b(0^+)$ in (9) is positive or negative, i.e., when $n_{2D} < \sigma_{\mathrm{pol}}$, the sign is "–," otherwise "+."

At this point, given that by definition $\varphi(0) = 0$ and considering (8) and (9), we define the parameter $C_o(n_{2D})$ as

$$C_o(n_{2D}) = \left(\frac{q(n_{2D} - \sigma_{\mathrm{pol}})}{\varepsilon_b}\right)^2 - \alpha\exp\left(-\frac{V_o(n_{2D})}{U_T}\right). \quad (10)$$

In (10), we highlighted the dependence of C on n_{2D} by noting $C_o(n_{2D})$.

We rewrite (8) as

$$\frac{\partial\varphi(z)}{\partial z} = -F_b(z) = \pm\sqrt{\alpha\exp\left(\frac{\varphi(z) - V_o}{U_T}\right) + C_o(n_{2D})}. \quad (11)$$

We separate potentials from coordinate in (11) and integrate from $z = 0^+$ to z, where z is any point inside the barrier

$$\int_{\varphi(0)=0}^{\varphi(z)} \frac{d\varphi(t)}{\sqrt{\alpha\exp\left(\frac{\varphi(t)-V_o(n_{2D})}{U_T}\right) + C_o(n_{2D})}} = \pm\int_0^z dt. \quad (12)$$

The integral in the LHS of (12) can be solved analytically, but the solution depends on the sign of $C_o(n_{2D})$. For a given polarization charge density σ_{pol}, the coefficient $C_o(n_{2D})$, as shown in (10), depends on n_{2D}, which in turn depends on the bias.

1) Solution When $C_o(n_{2D}) > 0$: Before proceeding toward the solution of (12), we focus on the resolution of the integral since this can be misleading. Applying two successive changes of variables, $y = \alpha\exp((\varphi - V_o)/U_T) + C_o(n_{2D})$ then $z = \sqrt{y}$, we can find that the arctanh function is the common solution proposed in textbooks. However, using the arctanh function implicitly assumes that the argument range is $[-1; 1]$, in contradiction with the term in the square root of (12) that is always

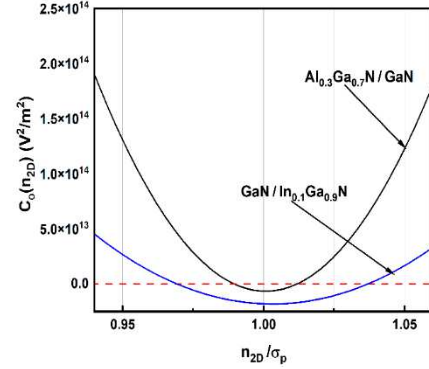

Fig. 2. Calculation of $C_o(n_{2D})$ for two heterostructures: $Al_{0.3}Ga_{0.7}N$/GaN and GaN/$In_{0.1}Ga_{0.9}N$.

greater than unity when $C_o(n_{2D}) > 0$. This contradiction can be removed by noting that the arccoth function is also a solution, while its argument range is $[-\infty; -1]U[1; \infty]$, compatible with our conditions. Therefore, the solution of (12) is

$$\frac{-2U_T}{\sqrt{C_o(n_{2D})}}\mathrm{acoth}\left(\sqrt{\frac{\alpha}{C_o(n_{2D})}e^{\frac{\varphi(z)-V_o(n_{2D})}{U_T}} + 1}\right)\Bigg|_0^{\varphi} = \pm z. \quad (13)$$

As we discussed for (8), when $n_{2D} > \sigma_{\mathrm{pol}}$, the positive sign is applied in the RHS of (13); otherwise, the negative sign must be used.

From relations (9), (11), and (13), for a given electron density in the QW n_{2D}, the electric field $F_b(z)$ in the barrier layer can be expressed with respect to z

$$F_b(z) = \sqrt{C_o(n_{2D})}\coth\left(\mathrm{acoth}\left(\frac{q(n_{2D} - \sigma_{\mathrm{pol}})}{\varepsilon_b\sqrt{C_o(n_{2D})}}\right) - \frac{\sqrt{C_o(n_{2D})}}{2U_T}z\right). \quad (14)$$

Since coth/arccoth functions are odd, relation (14) gives the correct sign of the electric field in the barrier that depends on whether n_{2D} greater than or lower than σ_{pol}.

2) Solution When $C_o(n_{2D}) < 0$: A trivial case for which C_o is negative when $qn_{2D} \approx \sigma_{\mathrm{pol}}$, i.e., when the polarization-induced fixed charges are compensated by the mobile 2-D charges in the QW.

When $C_o(n_{2D})$ is negative, integration of (12) gives

$$\frac{2U_T}{\sqrt{-C_o(n_{2D})}}\mathrm{atan}\left(\frac{\sqrt{\alpha e^{\frac{\varphi(z)-V_o(n_{2D})}{U_T}} + C_o(n_{2D})}}{\sqrt{-C_o(n_{2D})}}\right)\Bigg|_0^{\varphi} = \pm z. \quad (15)$$

As before, since tan/arctan functions are odd, relation (15) gives the correct sign of the electric field in the barrier

$$F_b(z) = \sqrt{-C_o(n_{2D})}\tan\left(z\frac{\sqrt{-C_o(n_{2D})}}{2U_T} + \mathrm{atan}\left(\frac{q(n_{2D} - \sigma_{\mathrm{pol}})}{\varepsilon_b\sqrt{-C_o(n_{2D})}}\right)\right). \quad (16)$$

To better illustrate the sign of $C_o(n_{2D})$, its dependence on the ratio $n_{2D}/\sigma_{\mathrm{pol}}$ is shown in Fig. 2 for $Al_{0.3}Ga_{0.7}N$/GaN and GaN/$In_{0.1}Ga_{0.9}N$ heterostructures.

We see that for practical values of n_{2D}, i.e., close to the polarization σ_{pol}, the coefficient $C_o(n_{2D})$ changes sign.

As we will see, the analyses of these two cases are necessary to predict the charge density from below to above threshold.

3) Potential Distribution in the Barrier: According to relation (11), the potential distribution $\varphi(z, n_{2D})$ for a given n_{2D} is

$$\varphi(z, n_{2D}) = U_T \ln\left[\frac{F_b(z, n_{2D})^2 - C_o(n_{2D})}{\alpha}\right] + V_o(n_{2D}) \quad (17)$$

where $F_b(z, n_{2D})$ is defined either by (14) or (16), depending on the sign of $C_o(n_{2D})$.

4) Asymptotic Maximum of n_{2D}: We now comment on how relations (13) and (15) predict an upper limit for the electron density in the QW (n_{2D_MAX}) for a given barrier thickness (d). To make this statement clear, we calculate the value of mobile charge density when the surface potential $\varphi(z = d)$ goes to infinity, which also means that the gate potential is infinite. Rewriting relations (13) and (15) while imposing $\varphi(d) \to \infty$, and noting that acoth$(\infty) \to 0$ and atan$(\infty) \to \pi/2$, we have

$$\frac{2U_T}{\sqrt{C_o(n_{2D})}} \text{acoth}\left(q\frac{n_{2D_max} - \sigma_{pol}}{\varepsilon_b\sqrt{C_o(n_{2D})}}\right) = d \quad \text{if } C_o > 0 \quad (18)$$

$$\frac{2U_T}{\sqrt{-C_o}}\left(\frac{\pi}{2} - \text{atan}\left(q\frac{n_{2D_max} - \sigma_{pol}}{\varepsilon_b\sqrt{-C_o(n_{2D})}}\right)\right) = d \quad \text{if } C_o < 0. \quad (19)$$

Equations (18) and (19) state that for an "infinitely high" voltage applied to the gate ($\varphi(d) \to \infty$), we expect an asymptotic maximum for the 2DEG density n_{2D_MAX} that can be generated in the QW for a given barrier thickness d.

While (18) and (19) are nonexplicit expressions for n_{2D_MAX} since $C_o(n_{2D})$ also depends on n_{2D_MAX}, we can substitute n_{2D} in (18) and (19) and calculate the corresponding thickness $z_{max}(n_{2D})$ as the largest thickness permitting the generation of the charge density n_{2D} in the QW.

According to (18) and (19), n_{2D_MAX} is defined by heterostructure material parameters but, most importantly, by the barrier layer thickness. In the case of high bandgap insulators, it is almost independent of the insulator layer properties and thickness.

This maximum 2DEG density corresponds to the onset of a marked increase of electrons density at the barrier/insulator interface. By screening the electric field, this electron "accumulation" weakens gate modulation of the channel potential and 2DEG density. As we will observe, numerical simulations predict that the charge density in the QW can still slightly increase beyond n_{2D_MAX} for a given barrier thickness when using Fermi–Dirac statistics in simulations. Unfortunately, introducing Fermi–Dirac statistics in our analytical approach prevents finding an analytical solution.

C. Including the Gate

Thus, the electrostatic analysis focused on the AlGaN–GaN heterostructure only, ignoring the gate insulator and the contact electrode. The gate potential is easily introduced by imposing the electrical displacement field continuity at the barrier/insulator interface ($z = d$) $E_i\varepsilon_i = F_b(d)\varepsilon_b$, where ε_i and E_i are the permittivity and the electric field (constant) in

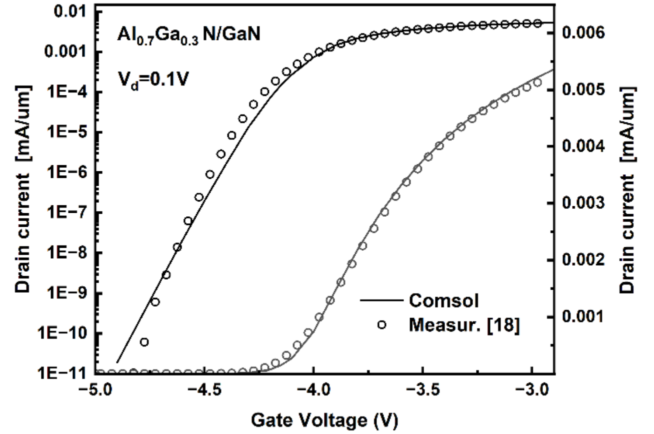

Fig. 3. Comparison of experimental data [18] with COMSOL simulations.

the insulator. Then, the effective gate potential is introduced as

$$V_G^* = t_i\frac{\varepsilon_b}{\varepsilon_i}F_b(d, n_{2D}) + \varphi(d, n_{2D}) \quad (20)$$

where $V_G^* = V_G - \Delta\psi_i$ having V_G as the gate voltage and $\Delta\psi_i$ as the work function difference between the insulator gate and the AlGaN layer, t_i is the insulator thickness, and $F_b(d, n_{2D})$ and $\varphi(d, n_{2D})$ are the electric field and potential at the barrier surface, respectively (note that in principle, the relationship between the voltages and the 2DEG density can be used to evaluate the drain current based on the equations presented in [27] that rely on source and drain charge densities. However, this is not at aim of this work.

It is important to note that the model remains valid whatever the nature of the gate electrode, i.e., metal–insulator or Schottky contact, provided a constant Fermi energy across the AlGaN–GaN heterostructure is satisfied.

III. Discussion

We present simulations on some relevant AlGaN HEMT structures and validate the results with COMSOL Multiphysics, which were also validated against experimental data. Concerning the analytical model, calculations have been performed in PTC Mathcad Prime 8.

The 2-D simulations were then tuned to match with experimental data provided by IMEC for MISHEMT. As described in [18], the devices consist of a 3-nm barrier layer with 70% aluminum content, followed by a 5-nm-thick Si_3N_4 insulating layer. Source and drain access regions were 0.75- and 1.5-μm length, respectively, and the gate length was 0.5 μm. The I–V transfer characteristics computed from simulations and extracted from experimental data are presented in Fig. 3.

Since in the model we focus on MISHEMT capacitors, we will rely on 1-D simulations, using the same setup validated for 2-D simulations. Three semiconductor heterostructures with different semiconductor compositions are investigated. For each case, the barrier thickness is varied.

The gate metal work function is set to 4.3 V, and then the work function difference ($\Delta\psi_i$) is calculated based on barrier layer material parameters presented in Table I.

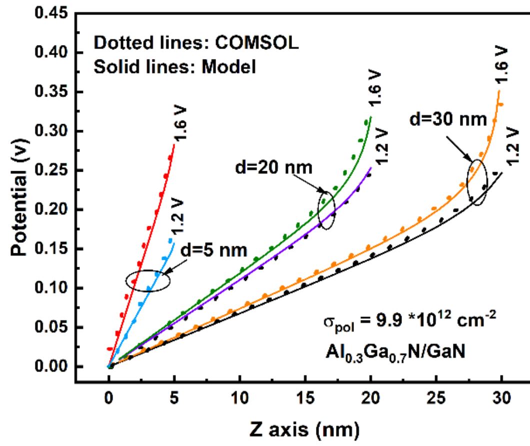

Fig. 4. Electric potential along the z-axis in the barrier for different barrier thicknesses and gate voltages.

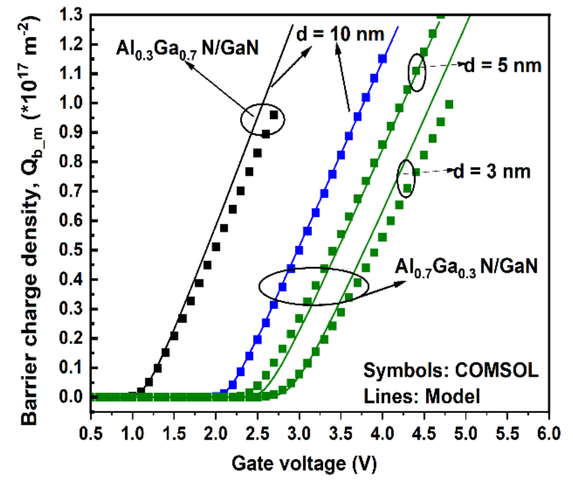

Fig. 5. Mobile charge density in $Al_xGa_{1-x}N$ barrier layer for $x = 0.3$ and $x = 0.7$ with different barrier thicknesses.

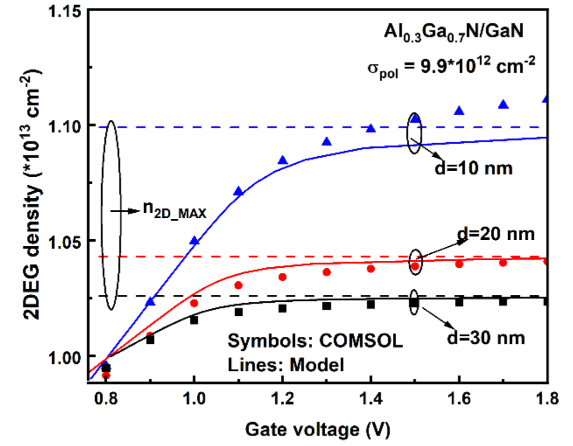

Fig. 6. 2DEG density versus gate voltage for 30-, 20-, and 10-nm barrier thicknesses.

We start the analysis with the $Al_{0.3}Ga_{0.7}N/GaN$ system. According to [4], the fixed polarization charge density σ_{pol} is 1.58×10^{-6} C/cm^{-2}, or equivalently 9.9×10^{12} cm^{-2} in terms of the elementary charge unit. Fig. 4 represents the potential distribution in the $Al_{0.3}Ga_{0.7}N$ barrier layer along the z-axis for different barrier thicknesses, namely, 30, 20, and 5 nm. In addition, two gate voltages (V_G = 1.2 and 1.6 V) are chosen well above of threshold voltage (−2 V for this structure) and close to the n_{2D} saturation voltage. The potential is calculated with (17), where $F_b(z, n_{2D})$ is defined from (14) or (16). The agreement between the analytical model and COMSOL simulation is confirmed (dots: COMSOL and lines: model). This photograph corresponds to the case where $n_{2D} > \sigma_{pol}$ (it will be shown that the condition $n_{2D} = \sigma_{pol}$, i.e., interface neutrality, for 30% Al content takes place at $V_G \approx 0.8$ V).

We observe a pronounced bending of the potential for barrier thicknesses of 20 and 30 nm that starts to rise sharply close to the barrier/insulator interface (note that $z = 0$ corresponds to the AlGaN/GaN interface). This variation gets more pronounced as the gate voltage is increased. From relation (1), the curvature of the potential means that a charge builds up in the layer and suggests that the AlGaN barrier cannot be treated anymore as an insulator, but behaves as a semiconductor. This is further confirmed in Fig. 5, where the mobile charge density in the AlGaN layer increases above a certain value of the gate voltage. This photograph looks like the characteristics of an MOS capacitor, except that the channel in our device is located at the AlGaN/GaN interface, i.e., d nanometers away from the AlGaN–insulator interface. The onset of charge enhancement in the barrier is higher for thicker barrier layers (see Fig. 5). The increase of gate voltage is causing accumulation of electrons in the whole barrier, but more specifically at barrier/insulator interface ($z = d$), as can be anticipated in Fig. 4 by the potential curvature near $z = d$ for different structures. However, when the barrier thickness is 5 nm, we observe a linear dependence of the potential with z, meaning that at this thickness accumulation of charges in the barrier reaches at higher voltages (see Fig. 5).

The density of 2DEG in the QW is plotted versus the gate voltages in Fig. 6 for different barrier thicknesses. For each barrier thickness, relation (18) predicts a maximum charge density in the QW. These maximum charge densities (n_{2D_MAX}) calculated from (18) are indicated with dashed lines. For 20- and 30-nm-thick barrier layers, the correspondence between the analytical model and COMSOL simulations is accurate, whereas for 10-nm-thick barrier, we start observing a slight mismatch at high voltages. This mismatch comes from the model limitation where we used Maxwell–Boltzmann distribution while at V_G = 1.4 V, the conduction band already crosses the electron quasi-Fermi at the edge of the AlGaN barrier. This situation also exists for thicker barrier layers; however, the ratio of the degenerated extension of the barrier with respect to the total thickness is smaller in that case, leading to a better matching between the model and simulations. It is interesting to note that the "saturation" of n_{2D} for the 10-nm barrier device, for instance (see Fig. 6), occurs at a gate voltage where the charge density in the barrier starts increasing, see the plot in Fig. 5 for 30% aluminum content. As we explained before, the excess charge in the barrier screens the gate potential at the AlGaN/GaN interface, i.e., in the QW.

The 2DEG density in the QW versus the gate voltage for thinner barrier layers (7, 5, and 3 nm) and for two aluminum contents of the AlGaN barrier, 30% and 70%, is shown in Fig. 7. The good agreement between the model

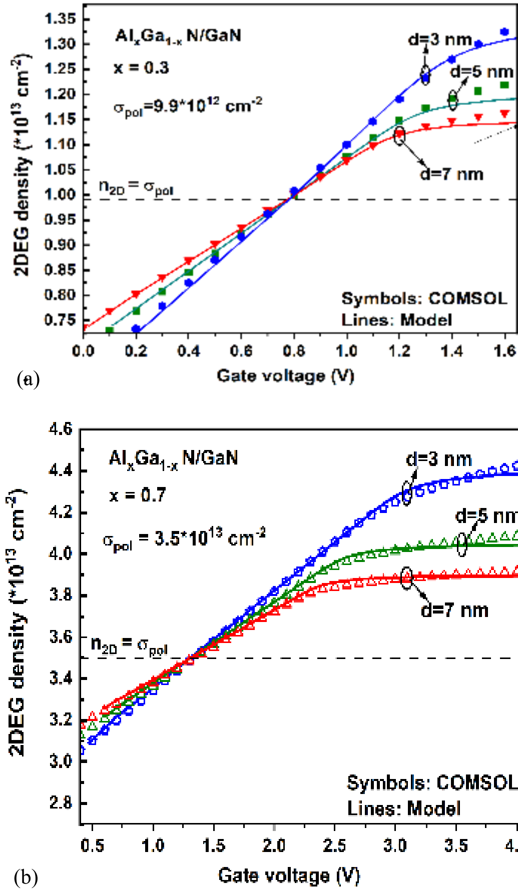

Fig. 7. 2DEG density versus the gate voltage for 7-, 5-, and 3-nm AlGaN barrier thicknesses, with aluminum content of (a) 30% and (b) 70%.

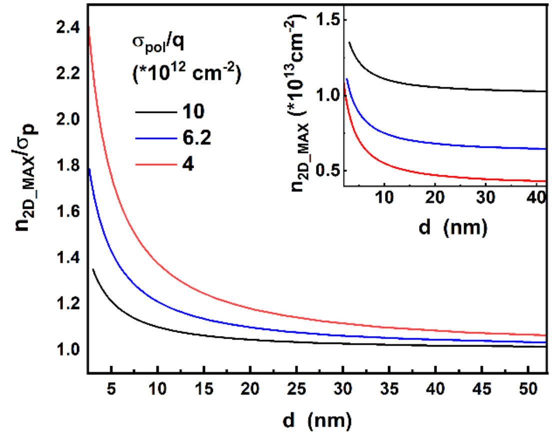

Fig. 8. Maximum 2DEG density normalized to the polarization charge density versus the barrier thickness for a different σ_{pol}. The inset illustrates the same plots with nonnormalized n_{2D_MAX}.

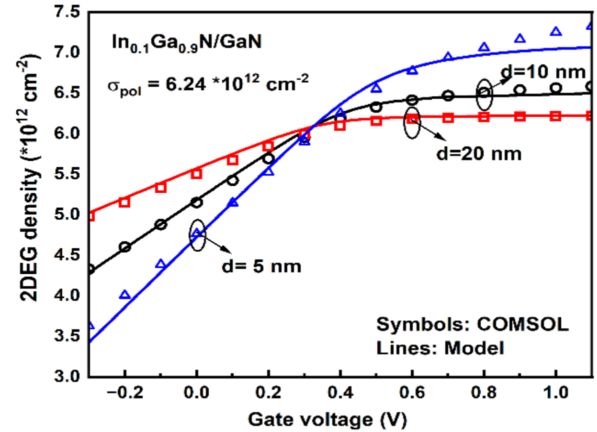

Fig. 9. 2DEG density versus gate voltage for 20-, 10-, and 5-nm GaN barrier thicknesses for GaN-/InGaN-MISHEMT.

and simulations for both barrier compositions supports the validity and soundness of our approach. Dashed lines, in either Fig. 7(a) or (b), indicate the position when the 2DEG density equals the polarization charge density ($n_{2D} = \sigma_{pol}$). Whatever the barrier thickness, all the curves cross at almost the same gate voltage that corresponds to the channel neutrality state at the heterojunction, i.e., $n_{2D} = \sigma_{pol}$. Below this value, the charge in the QW varies almost linearly with the gate voltage.

As we commented, for this range of bias, the barrier behaves as an insulator (no significant mobile charges in the barrier). When n_{2D} becomes higher than σ_{pol}, we observe the same trend as in Fig. 6, where the 2DEG tends to saturate, and this asymptote is very dependent on the barrier thickness.

The saturation in the QW predicted by relations (18) and (19) depends on the polarization charge σ_{pol}. This is illustrated in Fig. 8, where the "saturation," anticipated by the analytical model, is expressed as the maximum 2DEG density normalized to the polarization charge (n_{2D_MAX}/σ_{pol}) for a different σ_{pol}. We observe that the lower σ_{pol}, the higher n_{2D_MAX}/σ_{pol}. For instance, for a 5-nm barrier thickness imposing $\sigma_{pol} = 4 \times 10^{12}$ cm^{-2} predicts that n_{2D_MAX} is about $1.8\sigma_{pol}$, whereas when $\sigma_{pol} = 10^{13}$ cm^{-2}, the normalized saturation is lower, $n_{2D_MAX} \approx 1.2\sigma_{pol}$. For thick barriers, larger than 40 nm, n_{2D_MAX}/σ_{pol} is even close to unity, meaning that we can hardly exceed the polarization charge density in the QW, which is not the case for ultrathin AlGaN barriers.

To verify the model, we also investigated the GaN/$In_{0.1}Ga_{0.9}N$ heterostructure (note that GaN is now the barrier and InGaN is the small bandgap semiconductor). As for the AlN/GaN system, a polarization charge density σ_{pol}, estimated to 6.46×10^{12} cm^{-2} (in terms of elementary charge) [9], exists at the GaN/$In_{0.1}Ga_{0.9}N$ heterojunction. Fig. 9 shows the density of the 2DEG versus the gate voltage for 20-, 10-, and 5-nm GaN barrier thicknesses, below and above σ_{pol}. Still, the agreement between the analytical model and COMSOL simulations is good. As for the AlGaN system, well above the neutrality condition, a slight mismatch between the numerical simulations and the analytical model is observed for the thinner barrier layer (5 nm), which is again attributed to the use of Fermi–Dirac statistics in COMSOL, while Boltzmann statistics are used in the model.

IV. Conclusion

We proposed a physics-based analytical model that predicts the potential screening arising from the accumulation of electrons at the insulator-AlGaN barrier interface on the charge density in the QW of AlGaN-/GaN-MISHEMTs, a result that was not anticipated before. An explicit expression of the asymptotic mobile charge density involving the polarization

charge density and the barrier thickness was developed and validated by numerical simulations. It is likely that this work can be extended to predict the gate leakage current in GaN HEMT.

Appendix

The first excited state in GaN/AlGaN heterostructure lies mainly the above Fermi level, as evidenced in [1]. Since we consider only the ground state, as in [24], we introduce a correction factor C in the density of states in order to emulate the occurrence of the second confined level.

The 2DEG sheet density is then given by [1]

$$n_{2\text{D}} = \text{DOS}kT \ln\left(1 + \exp\left(\frac{E_F - E_o}{kT}\right)\right) \quad \text{(A1)}$$

where DOS $= C(m_{\text{eff_GaN}}/\pi\hbar^2)$ is the 2-D density of states, with $m_{\text{eff_1}}$ being the effective mass of electrons in GaN and $C = 1.1$ according to [24]. Referring to our reference energy level (the conduction band edge of GaN at the interface), we have $E_o = \alpha_q F(0^-)^{(2/3)}$, where $F(0^-)$ is the effective electric field in the QW and $\alpha_q = ((9\pi\hbar q/8(2m_{\text{eff_GaN}})^{1/2}))^{2/3}$. The experimental value for α_q is given in [29]. For undoped or unintentionally doped material, the effective field is $F(0^-) = (qn_{2\text{D}}/k\varepsilon_{\text{GaN}})$ [1], where k is a fitting parameter used to calculate the effective field from the surface electric field. The Femi level (E_F) is calculated from (A1) and is introduced in (6).

References

[1] M. S. Shur, "GaN and related materials for high power applications," *MRS Online Proc. Library*, vol. 483, pp. 15–26, Dec. 1997, doi: 10.1557/proc-483-15.

[2] Y.-F. Wu, D. Kapolnek, J. P. Ibbetson, P. Parikh, B. P. Keller, and U. K. Mishra, "Very-high power density AlGaN/GaN HEMTs," *IEEE Trans. Electron Devices*, vol. 48, no. 3, pp. 586–590, Mar. 2001, doi: 10.1109/16.906455.

[3] T. R. Lenka and A. K. Panda, "Characteristics study of 2DEG transport properties of AlGaN/GaN and AlGaAs/GaAs-based HEMT," *Semiconductors*, vol. 45, no. 5, pp. 650–656, May 2011, doi: 10.1134/s1063782611050198.

[4] O. Ambacher et al., "Two-dimensional electron gases induced by spontaneous and piezoelectric polarization charges in N- and Ga-face AlGaN/GaN heterostructures," *J. Appl. Phys.*, vol. 85, no. 6, pp. 3222–3233, Mar. 1999, doi: 10.1063/1.369664.

[5] E. T. Yu, G. J. Sullivan, P. M. Asbeck, C. D. Wang, D. Qiao, and S. S. Lau, "Measurement of piezoelectrically induced charge in GaN/AlGaN heterostructure field-effect transistors," *Appl. Phys. Lett.*, vol. 71, no. 19, pp. 2794–2796, Nov. 1997, doi: 10.1063/1.120138.

[6] C. E. Dreyer, A. Janotti, C. G. Van de Walle, and D. Vanderbilt, "Correct implementation of polarization constants in Wurtzite materials and impact on III-nitrides," *Phys. Rev. X*, vol. 6, no. 2, Jun. 2016, Art. no. 021038, doi: 10.1103/physrevx.6.021038.

[7] D. Yan, H. Lu, D. Cao, D. Chen, R. Zhang, and Y. Zheng, "On the reverse gate leakage current of AlGaN/GaN high electron mobility transistors," *Appl. Phys. Lett.*, vol. 97, no. 15, Oct. 2010, Art. no. 153503, doi: 10.1063/1.3499364.

[8] G. Li, Y. Cao, H. G. Xing, and D. Jena, "High mobility two-dimensional electron gases in nitride heterostructures with high Al composition AlGaN alloy barriers," *Appl. Phys. Lett.*, vol. 97, no. 22, Nov. 2010, Art. no. 222110, doi: 10.1063/1.3523358.

[9] H. Zhang, E. J. Miller, E. T. Yu, C. Poblenz, and J. S. Speck, "Measurement of polarization charge and conduction-band offset at $In_xGa_{1-x}N$/GaN heterojunction interfaces," *Appl. Phys. Lett.*, vol. 84, no. 23, pp. 4644–4646, Jun. 2004, doi: 10.1063/1.1759388.

[10] S. Khandelwal, N. Goyal, and T. A. Fjeldly, "A physics-based analytical model for 2DEG charge density in AlGaN/GaN HEMT devices," *IEEE Trans. Electron Devices*, vol. 58, no. 10, pp. 3622–3625, Oct. 2011, doi: 10.1109/TED.2011.2161314.

[11] K. Li and K. H. Teo, "Gate leakage mechanisms and modeling in GaN based high electron mobility transistors-literature survey," Mitsubishi Electr. Res. Laboratories, Cambridge, MA, USA, Tech. Rep., Dec. 2019. [Online]. Available: https://www.merl.com/publications/docs/TR2019-160.pdf

[12] S. Karboyan et al., "Influence of gate leakage current on AlGaN/GaN HEMTs evidenced by low frequency noise and pulsed electrical measurements," *Microelectron. Rel.*, vol. 53, nos. 9–11, pp. 1491–1495, Sep. 2013, doi: 10.1016/j.microrel.2013.07.020.

[13] D. Favero et al., "Trade-off between gate leakage current and threshold voltage stability in power HEMTs during ON-state and OFF-state stress," *Microelectron. Rel.*, vol. 150, Nov. 2023, Art. no. 115129, doi: 10.1016/j.microrel.2023.115129.

[14] K. Takakura et al., "Parasitic subthreshold drain current and low frequency noise in GaN/AlGaN metal-oxide-semiconductor high-electron-mobility field-effect-transistors," *Semicond. Sci. Technol.*, vol. 36, no. 2, Feb. 2021, Art. no. 024003, doi: 10.1088/1361-6641/abce8c.

[15] Y. Hao et al., "High-performance microwave gate-recessed AlGaN/AlN/GaN MOS-HEMT with 73% power-added efficiency," *IEEE Electron Device Lett.*, vol. 32, no. 5, pp. 626–628, May 2011, doi: 10.1109/LED.2011.2118736.

[16] Y. Yue et al., "AlGaN/GaN MOS-HEMT interfacial passivation layer grown by atomic layer deposition," *IEEE Electron Device Lett.*, vol. 29, no. 8, pp. 838–840, Aug. 2008.

[17] W. Chong, M. Xiaohua, F. Qian, H. Yue, Z. Jincheng, and M. Wei, "Development and characteristics analysis of recessed-gate MOS HEMT," *J. Semicond.*, vol. 30, no. 5, May 2009, Art. no. 054002.

[18] S. Yadav et al., "High performance mm wave AlN/GaN MISHEMTs on 200 mm Si substrate," in *IEDM Tech. Dig.*, Feb. 2023, pp. 1–4, doi: 10.1109/IEDM45741.2023.10413712.

[19] J. Zhang, B. Syamal, X. Zhou, S. Arulkumaran, and G. I. Ng, "A compact model for generic MIS-HEMTs based on the unified 2DEG density expression," *IEEE Trans. Electron Devices*, vol. 61, no. 2, pp. 314–323, Feb. 2014, doi: 10.1109/TED.2013.2295400.

[20] C.-Y. Huang, S. Mazumder, P.-C. Lin, K.-W. Lee, and Y.-H. Wang, "Improved electrical characteristics of AlGaN/GaN high-electron-mobility transistor with Al_2O_3/ZrO_2 stacked gate dielectrics," *Materials*, vol. 15, no. 19, p. 6895, Oct. 2022, doi: 10.3390/ma15196895.

[21] Z.-E. Touati, Z. Hamaizia, and Z. Messai, "DC and RF characteristics of AlGaN/GaN HEMT and MOS-HEMT," in *Proc. 4th Int. Conf. Electr. Eng. (ICEE)*, Dec. 2015, pp. 1–4, doi: 10.1109/INTEE.2015.7416850.

[22] X. Liu et al., "AlGaN/GaN metal-oxide-semiconductor high-electron-mobility transistor with polarized P(VDF-TrFE) ferroelectric polymer gating," *Sci. Rep.*, vol. 5, no. 1, p. 14092, Sep. 2015, doi: 10.1038/srep14092.

[23] T. Ueda, "GaN power devices: Current status and future challenges," *Jpn. J. Appl. Phys.*, vol. 58, Jun. 2019, Art. no. SC0804, doi: 10.7567/1347-4065/ab12c9.

[24] H. Yu et al., "Surface state spectrum of AlGaN/AlN/GaN extracted from static equilibrium electrostatics," *IEEE Trans. Electron Devices*, vol. 68, no. 11, pp. 5559–5564, Nov. 2021, doi: 10.1109/TED.2021.3115086.

[25] X.-G. He, D.-G. Zhao, and D.-S. Jiang, "Formation of two-dimensional electron gas at AlGaN/GaN heterostructure and the derivation of its sheet density expression," *Chin. Phys. B*, vol. 24, no. 6, Jun. 2015, Art. no. 067301.

[26] D. Delagebeaudeuf and N. T. Linh, "Metal-(n) AlGaAs-GaAs two-dimensional electron gas FET," *IEEE Trans. Electron Devices*, vol. ED-29, no. 6, pp. 955–960, Jun. 1982, doi: 10.1109/T-ED.1982.20813.

[27] F. Jazaeri and J.-M. Sallese, "Charge-based EPFL HEMT model," *IEEE Trans. Electron Devices*, vol. 66, no. 3, pp. 1218–1229, Mar. 2019, doi: 10.1109/TED.2019.2893302.

[28] J. Qin, Q. Zhou, B. Liao, and H. Wang, "Modeling of 2DEG characteristics of $In_xAl_{1-x}N$/AlN/GaN-based HEMT considering polarization and quantum mechanical effect," *Electronics*, vol. 7, no. 12, p. 410, Dec. 2018, doi: 10.3390/electronics7120410.

[29] H. K. Kwon et al., "Radiative recombination of two-dimensional electrons in a modulation-doped Al_0.37Ga_0.63N/GaN single heterostructure," *Appl. Phys. Lett.*, vol. 75, no. 18, pp. 2788–2790, Nov. 1999, doi: 10.1063/1.125150.

[30] A. Goyal, A. K. Kapoor, R. Raman, S. Dalal, P. Mohan, and R. Muralidharan, "Band gap bowing parameter in pseudomorphic $Al_xGa_{1-x}N$/GaN high electron mobility transistor structures," *J. Appl. Phys.*, vol. 117, no. 22, p. 25702, Jun. 2015.

[31] I. P. Smorchkova et al., "Polarization-induced charge and electron mobility in AlGaN/GaN heterostructures grown by plasma-assisted molecular-beam epitaxy," *J. Appl. Phys.*, vol. 86, no. 8, pp. 4520–4526, Oct. 1999.